Journal of Orthopaedic Translation 52 (2025) 167–181

Contents lists available at ScienceDirect

Journal of Orthopaedic Translation

journal homepage: www.journals.elsevier.com/journal-of-orthopaedic-translation

Original Article

MAGI1 attenuates osteoarthritis by regulating osteoclast fusion in subchondral bone through the RhoA-ROCK1 signaling pathway

Jing Zhang [a,1], Wenhui Hu [b,c,1], Yuheng Li [c], Fei Kang [c], Xuan Yao [d], Jianmei Li [c,*], Shiwu Dong [c,e,**]

[a] College of Bioengineering, Chongqing University, Chongqing, 400044, PR China
[b] Department of Basic Medicine, Frontier Medical Service Training Brigade, Army Medical University (Third Military Medical University), Changji, Xinjiang, 831200, PR China
[c] Department of Biomedical Materials Science, College of Biomedical Engineering, Army Medical University (Third Military Medical University), Chongqing, 400038, PR China
[d] Department of Clinical Hematology Faculty of Laboratory Medicine, Army Medical University (Third Military Medical University), Chongqing, 400038, PR China
[e] State Key Laboratory of Trauma and Chemical Poisoning, Army Medical University (Third Military Medical University), Chongqing, 400038, PR China

ARTICLE INFO

Keywords:
Osteoarthritis
Subchondral bone
Osteoclast fusion
MAGI1
RhoA/ROCK1 signaling

ABSTRACT

Background: Osteoarthritis (OA) is a chronic joint disorder that predominantly affects middle-aged or elderly individuals. Subchondral bone remodeling due to osteoclast hyperactivation is regarded as a major feature of early OA. During osteoclast fusion and multinucleation, the cytoskeleton reorganization leads to the formation of actin belts and ultimately bone resorption. Membrane-associated guanylate kinase with an inverted repeat member 1 (MAGI1) is a scaffolding protein that is crucial for linking the extracellular environment to intracellular signaling pathways and cytoskeleton. However, the role of MAGI1 in subchondral bone osteoclast fusion remains unclear.

Methods: In this study, we collected knee joint samples from OA patients and established the OA mouse model to examine the expression of MAGI1. Furthermore, we established the OA rat model and locally injected rAAV9-mediated shMagi1 into the subchondral bone to knock down MAGI1 expression. Micro-CT, histological staining, and immunofluorescence were employed to assess the effects of MAGI1 knockdown on subchondral bone homeostasis and OA process. We isolated and cultured osteoclasts from femoral and tibial bone marrow. Receptor activator of nuclear factor-κB ligand (RANKL)-stimulated osteoclasts served as an *in vitro* model for OA and underwent RNA sequencing. We employed gain- and loss-of-function experiments using MAGI1-overexpression plasmids and small interfering RNA to explore the role of MAGI1 in osteoclast differentiation. Further molecular experiments, including RT-qPCR, western blotting, immunofluorescence staining, and LC-MS/MS were performed to investigate underlying mechanisms.

Results: MAGI1 expression was significantly downregulated during RANKL-induced osteoclastogenesis *in vitro*. Additionally, a progressive decrease in MAGI1 expression was consistently observed in both knee joint samples from OA patients and mouse OA models, correlating with OA progression. Knockdown of MAGI1 in subchondral bone increased osteoclast numbers and worsened subchondral bone microarchitecture and cartilage degeneration; MAGI1 knockdown rats exhibited elevated PDGF-BB, Netrin-1, and $CGRP^{+}$ sensory innervation. Overexpression and knockdown of MAGI1 suppressed and promoted osteoclast differentiation, respectively. Mechanistically, MAGI1 overexpression decreased the levels of RhoA, ROCK1, and p-p65 in RANKL-treated osteoclasts, which was rescued by the addition of RhoA activator narciclasine.

Conclusion: Our results demonstrate that MAGI1 suppresses osteoclast fusion through the RhoA/ROCK1 signaling pathway, targeting MAGI1 in subchondral bone osteoclasts may be a promising therapeutic strategy mitigate the advancement of OA.

* Corresponding author.
** Corresponding author. Department of Biomedical Materials Science, College of Biomedical Engineering, Army Medical University (Third Military Medical University), Chongqing 400038, PR China.
E-mail addresses: lijianmei@tmmu.edu.cn (J. Li), dongshiwu@tmmu.edu.cn (S. Dong).
[1] The first two authors (Jing Zhang and Wenhui Hu) contributed equally to this work.

https://doi.org/10.1016/j.jot.2025.04.007
Received 10 December 2024; Received in revised form 30 March 2025; Accepted 14 April 2025

The translational potential of this article: This study reveals that the scaffold protein MAGI1 participates in osteoarthritis progression by regulating osteoclast fusion, providing novel theoretical foundations and potential therapeutic targets for osteoarthritis treatment.

1. Introduction

Osteoarthritis (OA) is a chronic degenerative joint disease that causes joint pain and stiffness [1]. According to estimates in 2020, approximately 240 million individuals worldwide suffering from symptomatic OA [2]. Currently, total joint replacement is a major breakthrough in the treatment of advanced OA, but there is lack of effective treatments for early and intermediate OA, with an important reason that the cellular and molecular mechanism of OA has not been fully elucidated [3–5]. Thus, a deeper understanding of the pathogenesis of early-stage OA to support novel therapeutic strategies is urgently necessary.

The characterized features in OA are articular cartilage degeneration, subchondral bone remodeling, synovial inflammation, and formation of osteophytes [6]. Recently, an increasing number of researches support that pathologic changes in subchondral bone play a key role in the progression of OA and that alterations in subchondral bone microarchitecture appear prior to articular cartilage damage [7–9]. Articular cartilage and subchondral bone function together in a normal joint, facilitating the transfer of pressure from the cartilage to the subchondral bone below. However, abnormal mechanical stimulation causes osteoclasts to be overactivated, contributing to uncoupling of bone remodeling and damage to the microstructure of subchondral bone [10]. In the early murine OA models, the number of osteoclasts in the subchondral bone is significantly increased, overactivation of osteoclast releases various cytokines such as transforming growth factor β1 (TGF-β1) and platelet-derived growth factor-BB (PDGF-BB), which in turn regulate the homeostasis of cartilage [11,12]. Furthermore, TGF-β1 and PDGF-BB promote type H vascularization of subchondral bone in the early-stage OA, which further disrupt the remodeling of subchondral bone [11,13,14]. Moreover, subchondral bone may also be an important source of pain in OA, overactivated osteoclasts secrete Netrin-1 and play a central role in pain hypersensitivity mediating by calcitonin gene-related peptide (CGRP) positive sensory nerve fibers innervation in subchondral bone [15,16]. Hence, targeting subchondral bone osteoclasts to find therapeutic options for the treatment of OA is necessary.

Membrane-associated guanylate kinase, WW and PDZ domain-containing protein (MAGI) is a subfamily within the membrane-associated guanylate kinase (MAGUK) family [17]. Research has revealed that the MAGI family comprises three members: MAGI1, MAGI2, and MAGI3 [18]. Among the three members of the MAGI family, MAGI1 was discovered in 1998 and was initially described as an intracellular scaffolding protein involved in stabilizing epithelial cell junctions [19]. With the deepening of research, an increasing number of studies indicated that MAGI1 participates in diverse fundamental biological processes, including regulating cell–cell and cell–matrix adhesion, signal transduction, cell proliferation, and migration [20]. Thus, MAGI1 is becoming crucial for linking the extracellular environment to intracellular signaling pathways and cytoskeleton at synapses and tight junctions [21]. In cancer cells, MAGI1 acts as a tumor suppressor, studies have shown that MAGI1 inhibits p38 activity by releasing actin strength in luminal breast cancer and in experimental colon cancer [22]. MAGI1 has tumor suppressor and anti-metastatic activities through inhibiting the Wnt/β-catenin signaling pathway [23]. Moreover, in endothelial cells, MAGI1 is reported to stabilize cell adhesion by activating Rap1 [24], and endothelial cell-specific transgenic expression of MAGI1 increased NO production *ex vivo* in isolated endothelial cells by inducing PKA and eNOS phosphorylation [25].

Noteworthily, osteoclast formation is an intricate process of differentiation from monocytes/macrophages to mature osteoclasts, including a differentiation phase followed by a fusion stage and a multinuclear stage. Classically, osteoclast fusion consists of four basic steps: cell migration, recognition, cell–cell adhesion, and membrane fusion [26]. Dynamic rearrangement of the cytoskeleton and cytoplasmic membrane is required in these processes [27]. This reorganization is mediated by the formation of actin-rich structures, specifically filopodia and podosomes [28,29]. During the process of osteoclast fusion, filopodia sense extracellular stimuli, facilitate migration, and initiate cell–cell fusion [29–31]. Mature osteoclasts subsequently migrate and attach to the bone matrix surface, where podosomes undergo reorganization to form stable sealing zones and ruffled borders that mediate bone resorption [32,33]. Hence, considering that the MAGI family is involved in physiological processes such as cell fusion, migration, and adhesion, whether MAGIs play a role in osteoclast differentiation aroused our interest.

In this research, we first demonstrated that MAGI1 expression was significantly downregulated during osteoclastogenesis. Additionally, a progressive decrease in MAGI1 expression was consistently observed in both knee joint samples from OA patients and mouse OA models, correlating with the progression of OA pathology. Furthermore, we found that siRNA-mediated MAGI1 knockdown in osteoclast promoted osteoclast fusion and multinucleation and MAGI1 silence in subchondral bone by recombinant adeno-associated virus serotype 9 (rAAV9)-mediated shRNA exacerbated damage of subchondral bone microstructure in OA rats. Whereas overexpression of MAGI1 significantly inhibits osteoclast formation. For the mechanism, MAGI1 downregulated the RhoA/ROCK1 signaling pathway and thus suppressed RANKL-induced NF-κB p65 phosphorylation. Thus, targeting MAGI1 in subchondral bone osteoclasts might offer a promising therapeutic strategy mitigate the advancement of OA.

2. Materials and methods

2.1. Chemicals and materials

α-Minimum Eagle's Medium (α-MEM) and fetal bovine serum (FBS) were obtained from Gibco (Grand Island, NY, USA). Recombinant murine macrophage colony-stimulating factor (M-CSF) and recombinant murine RANKL were acquired from R&D Systems (Minneapolis, MN, USA). Cell Counting Kit-8 (CCK-8) was supplied by Beyotime (Shanghai, China). Tartrate-resistant acid phosphatase (TRAP) kit was provided by Sigma–Aldrich (St. Louis, MO, USA). Narciclasine (Narc) was purchased from MCE (Shanghai, China). Matrigel matrix gel was obtained from BD (Bedford, MA, USA).

2.2. Collection of clinical samples from OA patients

All samples were obtained from the Department of Orthopedics at Xinqiao Hospital of Army Medical University. This study was approved by the Medical Ethics Committee of Xinqiao Hospital, Army Medical University (Ethics Review No.: Research 056-01), and informed consent was obtained from all patients and their families. All samples were collected from OA patients undergoing knee replacement surgery. The patients were aged 58–79 years and had no history of major diseases such as malignant tumors.

2.3. Establishment of the DMM-induced OA mouse/rat model

We purchased 10-week-old C57BL/6J male mice and Sprague–Dawley male rats from Vital River Laboratory Animal Technology

Co., Ltd (Beijing, China). The mice and rats were housed in the Animal Experiment Center of Army Medical University, and housed under specific pathogen free (SPF) and germ-free (GF) conditions.

Grouping of mice: the mice were randomly divided into two groups: Sham group and Destabilization of the medial meniscus (DMM) group (n = 5 per group). Grouping of rats: the rats were randomly divided into two groups: Sham group and DMM group (n = 10 per group). One week after the establishment of the DMM model, the rats in both Sham group and DMM groups were subdivided into two subgroups: the AAV-con group and the AAV-shMagi1 group, with 5 rats per subgroup.

OA models induced by DMM was set up as the previously description [34]. Briefly, after mice and rats were anesthetized by an intraperitoneal injection using 1 % pentobarbital sodium (40 mg/kg), DMM surgery was performed on the right knee joint sectioning the medial meniscus ligament between the medial meniscus and tibial plateau. The sham group followed the same procedure without ligament sectioning. Four weeks after surgery, mice were sacrificed for further experiments. All animal experiments received approval from the Ethics Committee of Third Military Medical University (AMUWEC2019235). The study adhered to all relevant ethical guidelines for animal research and testing.

2.4. Gait analysis

Using the automated gait analysis hardware (Catwalk XT 10.5, Noldus) to collect the mice gaits as previously described [35]. The mice are placed at one end of the walkway so that they naturally walk through the glass channel without being forced. During the movement, a high-speed camera can clearly capture the footprint information of the mice during the walking process. The gait analysis system can automatically identify and analyze multiple indicators of the mice's footprints. The max contact max intensity (maximum intensity at the maximum contact of a paw), print area, and stride length of the right hind paws were selected for statistical analysis.

As previously described [36], to assess changes in the gait of rats, the left and right hide paws were coated with two non-toxic water-soluble color inks (left hide paws: blue, right hide paws: red). The rats walk along a 100-cm-long, 15-cm-wide runway and the floor of the runway was covered with sheets of white paper. The stride length and print area of the right hind paws were statistically analyzed.

2.5. Micro-computed tomography analysis

We fixed knee joints samples with 4 % solution of paraformaldehyde and scanned the joints using Micro-CT (Skyscan 1172; Bruker Micro-CT, Belgium). The scanning parameter were set as following: resolution, 10 μm/pixel, 70 kV and 200 μA. We reconstructed and analyzed the images using NReconServerLocal64 and CTAn64, respectively. The CTVol v2.0 software for three-dimensional model visualization was utilized to examine the parameters of trabecular bone in the metaphysis. We started counting from the medial aspect of the joint, defined the presence of subchondral bone tissue as the first image, and then selected 150 consecutive images to identify the region of interest (ROI). Three-dimensional structural parameters analyzed included: trabecular bone volume per tissue volume (BV/TV), trabecular thickness (Tb.Th), trabecular number (Tb.N), and trabecular separation (Tb. Sp).

2.6. Histochemistry and immunofluorescence

All knee samples were decalcified with 10 % ethylenediaminetetraacetic acid (EDTA) for at least 3 weeks. The samples were embedded in paraffin and were consecutively sectioned with thickness of 4 μm. Then, safranine O-fast green (SO-FG), hematoxylin & eosin (H&E), and TRAP staining was performed according to the standard operation procedures [37], and the image results were obtained through an inverted microscope. Cartilage damage degradation was assessed according to the OA Research Society International (OARSI) cartilage classification system. Subchondral bone damage was evaluated based on the TRAP staining results.

To detect the expression of MAGI1, PDGF-BB, and CGRP in the subchondral bone region, we performed immunofluorescence tests following the standard procedures. Briefly, after incubating the sections with primary antibodies overnight at 4 °C, and then secondary antibodies were applied at room temperature. Antibodies for immunostaining are detailed in Supplementary Table 3. The fluorescence signal intensity was analyzed using Image J software.

2.7. Local injection of rAAV9 in subchondral bone

rAAV9 carrying Magi1 shRNA was locally injected into the subchondral bone region to silence MAGI1 expression. Briefly, DMM surgery and sham operation were carried out on the right knee of 10-week-old SD rats. One-week post-surgery, 1.5×10^{11} AAV particles were injected into the subchondral bone of the right knee of SD rats treated with DMM and sham surgery. The injection procedure was conducted as follows: X-ray imaging was used to confirm the precise positioning of the injection needle to ensure accurate delivery. After exposing the knee joint, a puncture needle was inserted into the tibial plateau, followed by the advancement of a fine needle through the puncture needle into the subchondral bone region for AAV delivery. To avoid injection into the joint cavity, the needle was advanced slowly during the procedure. The Magi1 shRNA virus (rAAV9-U6-CMV-GFP-shMagi1) and the control (rAAV9-CMV-GFP) were constructed by Pai Wei Bio-Technology (Wuhan, China). The target sequence of Magi1 shRNA was 5-CACC-CAGCCAGAGCUAAUAAC-3, and the control was AAV9-CMV-GFP. The Magi1 shRNA sequence was inserted into the intron of the U6 promoter to drive the expression of GFP, which was utilized to detect AAV induced Magi1 shRNA expression.

2.8. Extraction and culture of BMDMs

Bone marrow-derived monocytes (BMDMs) were flushed from femoral and tibial bone marrow of 6-week-old C57BL/6 male mice and cultured with previously reports [38]. For osteoclast differentiation, BMDMs were cultured with α-MEM medium supplemented with M-CSF (50 ng/ml) and RANKL (100 ng/ml) for 5–6 days. Culture medium was replaced every other day until mature osteoclasts had formed. Osteoclast formation was assessed using TRAP staining as per the guidelines provided by Sigma-Aldrich [38]. TRAP-positive cells with more than three nuclei were identified as mature osteoclasts, using bright-field light microscope (Leica Microsystems, Wetzlar, Germany) to measure osteoclasts number of per well.

2.9. Cell transfection

Small interfering RNA (siRNA) and overexpression plasmids were provided by Genechem (Shanghai, China). BMDMs were transfected using lipofectamine 3000 (Invitrogen). Briefly, BMDMs were seeded in 6-well plates at a density of about 20,000 cells/well, and siRNAs and plasmids were transfected with Opti-MEM (Gibco) after 24 h of BMDMs adherence. After 6 h of transfection, the medium was replaced with normal α-MEM. After 48 h, the efficiency of transfection was verified by RT-qPCR and western blotting. Transfected BMDMs were then treated with M-CSF and RANKL to differentiate into osteoclasts for further analysis. The sequences of the siRNAs are listed below:

siRNA#1: 5′-CGCACAAUCAAGUCGUGGAUA-3′
siRNA#2: 5′-CACAUGCUCAAGUUGUGAATT-3′
siRNA#3: 5′-CACCCAGCCAGAGCUAAUAAC-3′

2.10. Tube formation experiment

Conditioned media of siRNA-mediated MAGI1 knockdown and control group were collected and then used to induce human umbilical

vein endothelial cells (HUVECs) tube formation. Specifically, 100 μL of matrix glue (BD) was added to the 96-well plate. HUVECs (2×10^4 cells per well) were seeded on polymerized Matrigel after the matrix glue solidified. After incubation at 37 °C for 4–6 h, Cells were connected into tubular structures, which were then observed and photographed under a microscope. Image J was used to measure the cumulative branching length and number of tube nodes.

2.11. Filopodia and actin ring staining

BMDMs were seeded in 96-wells plates and induced to mature osteoclasts for 3 days. Then, as the previously description [39], F-actin rings were stained with FITC-labeled phalloidin, and MAGI1 was stained with anti-MAGI1 antibody. The nuclei were stained with DAPI. Finally, the cells were imaged by laser confocal microscopy and the filamentous feet were counted. After the cells treated with M-CSF and RANKL for 6 days, F-actin rings were stained with FITC-labeled phalloidin and the nuclei were stained with DAPI. Cells were photographed under a fluorescence microscope and F-actin rings statistics were performed.

2.12. LC–MS/MS analysis

RAW246.7 cells were treated with RANKL (100 ng/ml) for 2 days, and then the total lysates of the cells were collected and incubated with MAGI1 antibody for immunoprecipitation. The MAGI1-conjugated immunoprecipitants were analyzed by LC-MS/MS for protein peptide identification (Gene Sci-Tech). Finally, Protein Pilot software v4.0 (Applied Biosystems) was used to convert the raw data (.wiff) into peak lists (.mgf), and the peak lists was imported into Mascot software to search and match with the sequences in the database, so as to obtain the protein identification results.

2.13. Co-immunoprecipitation assay

Cells were lysed by cold IP-lysis buffer (50 mM Tris–HCl, 150 mM NaCl, 2 mM EDTA, 0.5 % NP40, pH 7.5) containing protease inhibitors (1 mM PMSF) and phosphatase inhibitor for 30 min as described previously [40]. The supernatant was obtained after homogenization and centrifugation, 20 μl was taken as the input group. Then, 500 μl of antibody dilution (20 μg/ml) was added to 50 μl of 50 % Protein A/G magnetic beads, and normal IgG of the same antibody species was used as a negative control, and the mixture was rotated at 25 °C for 1 h. Subsequently, cell lysate (5 mg/copy) was added to the Protein A/G magnetic beads antibody complex, and the mixture was rotated at 4 °C overnight. After washing the IP complex, 100 μl of 2 × SDS sample loading buffer was added, and the magnetic beads were separated with a magnetic rack, retaining the supernatant. Finally, the total cell protein, IgG eluted samples, and IP eluted samples were subjected to Western blotting detection of the target bands.

2.14. Statistical analysis

Each experiment was repeated at least three times. The data from our research were expressed as mean ± standard deviation (s.d.), and we performed statistical analysis using GraphPad Prism 8 software (GraphPad Software, San Diego, USA). Statistically, to compare two groups, Student's *t*-tests were employed, whereas one-way ANOVA was utilized for comparisons involving three or more groups. Statistical significance was defined as $P < 0.05$ ($^*P < 0.05$, $^{**}P < 0.01$, $^{***}P < 0.001$).

3. Results

3.1. The downregulation of MAGI1 is associated with increased osteoclast activity in subchondral bone of OA mice

To investigate the changes of cellular phenotype during differentiation of osteoclast from subchondral bone in the OA environment, we performed the transcriptome sequencing analysis of RANKL-induced primary osteoclasts samples together with the control samples. The results of Gene Ontology (GO) enrichment analysis showed that cytoskeletal reorganization (cytoskeleton organization, microtubule cytoskeleton organization, and actin cytoskeleton organization) and cell adhesion were highly correlated with osteoclast differentiation (Supplementary Fig. S1A). The Kyoto Encyclopedia of Genes and Genomes (KEGG) pathway also suggested focal adhesion and cell adhesion molecules involved in osteoclast differentiation (Supplementary Fig. S1B). As a scaffold protein localized at cell-cell junctions, MAGI1 plays a critical role in regulating cell–cell contacts. It has also been shown in cancer cells that the abnormal expression of MAGI1 influences the cell adhesion and invasiveness [21]. Considering the critical role of MAGI1 in cell migration and cell adhesion, we induced the BMDMs to differentiate into osteoclasts over various time intervals, RT-qPCR was employed to detect the transcriptional levels of MAGI family genes and osteoclast differentiation-related marker genes. The results revealed that the expression of MAGI family genes Magi1, 2, and 3 were down-regulated, contrary to the expression pattern with Acp5, Nfatc1, c-Fos, Dc-stamp, Atp6v0d2, and Ctsk during osteoclastogenesis. Noteworthily, Magi1 had the most significant downward trend among the MAGI family genes (Fig. 1A and B). Moreover, we stimulated the BMDMs with M-CSF and RANKL. TRAP staining and immunofluorescence co-localization of MAGI1 and F-actin were then performed. The results demonstrated that MAGI1 expression was down-regulated during osteoclast formation (Fig. 1C, D and Supplementary Fig. S1C). To further investigate the role of MAGI1 in the pathology of subchondral bone in OA, we collected joint samples from OA patients, which included OA regions with varying degrees of bone damage. SO-FG staining was conducted to evaluate the extent of damage in the cartilage and subchondral bone within the samples (Fig. 1E). Subsequently, we performed immunofluorescence co-staining of MAGI1 and TRAP to detect the alterations of MAGI1 expression. The results showed that MAGI1 was expressed in both groups of joint samples and was significantly downregulated in the osteoarthritic part of the human subchondral bone compared with the relatively normal (RN) part (Fig. 1F and G). Correspondingly, the expression of MAGI1 in the subchondral bone tissue was also examined. We established the DMM-induced OA mice model, SO-FG and TRAP staining showed slight damage in cartilage 4 weeks after DMM surgery and a significant increase of TRAP-positive osteoclasts number in the subchondral bone (Fig. 1H–J and K). Furthermore, immunofluorescence co-staining of MAGI1 and TRAP revealed that MAGI1 protein levels (green) exhibited a decreased trend in subchondral bone of DMM mice at 4 weeks post-surgery compared to the Sham group. This down-regulation of MAGI1 was accompanied by an increase in TRAP-positive osteoclasts (red), indicating enhanced osteoclast activity in the DMM group (Fig. 1I and L). In addition, the expression of MAGI1 in $TRAP^+$ multinucleated osteoclasts was lower than that in $TRAP^+$ mononuclear osteoclasts (Supplementary Figs. S1D and E). Taken together, these results demonstrate a significant link between downregulated MAGI1 expression and elevated osteoclast activity during OA progression.

3.2. MAGI1 knockdown mediates osteoclast fusion by enhancing the formation of filopodia in intro

Since MAGI1 expression is downregulated during osteoclast differentiation, we speculated that MAGI1 may play a key role in osteoclastogenesis. To confirm this hypothesis, we transiently transfected primary BMDMs using small interfering RNA (siRNA). Western blotting

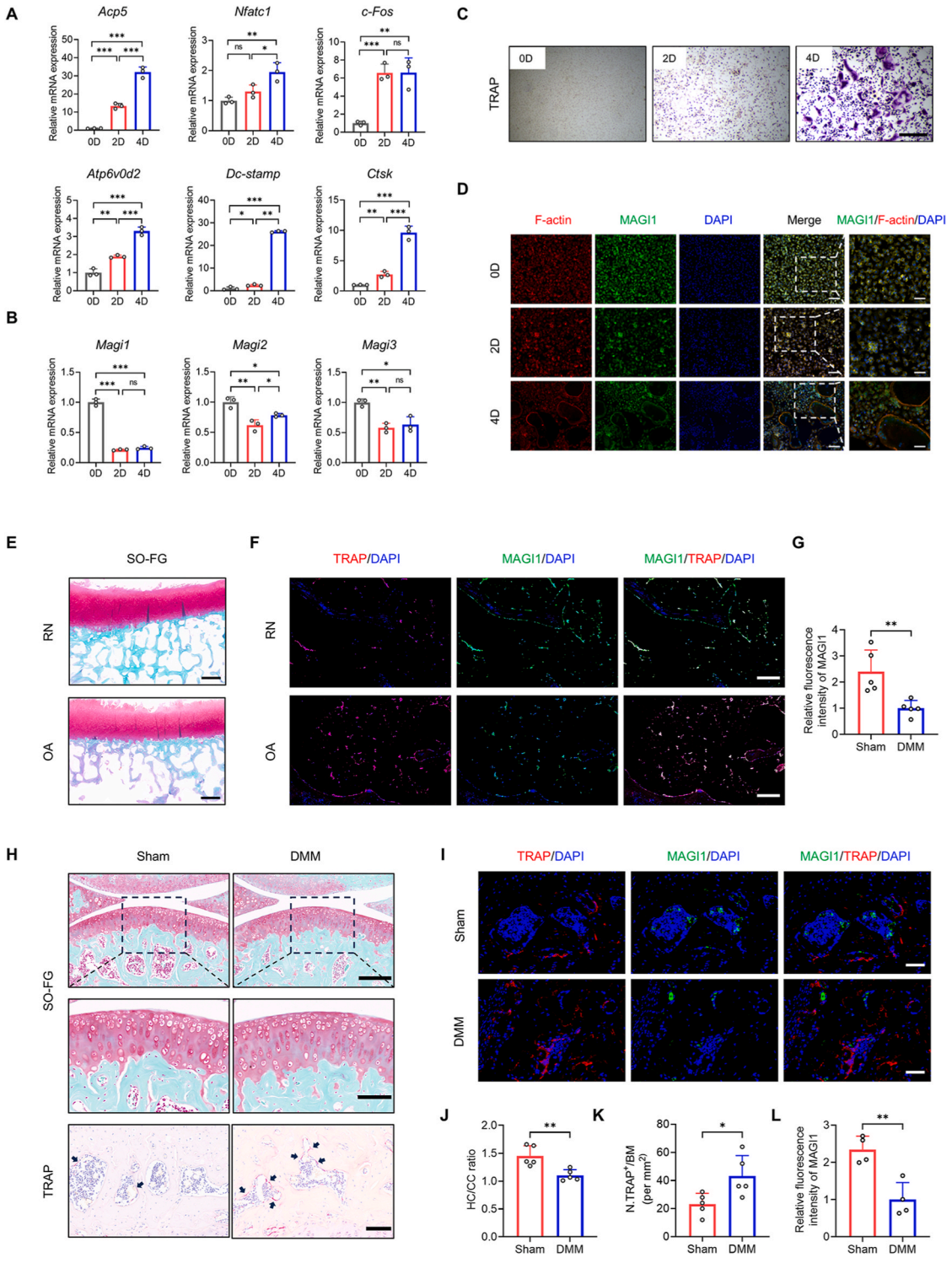

Fig. 1. MAGI1 expression in osteoclasts is correlated with the progression of OA. (A, B) RT-qPCR analysis of the expression of osteoclasts marker genes and MAGI family genes in BMDMs during RANKL-induced osteoclastogenesis at 0, 2 and 4 d n = 3. **(C)** TRAP staining of osteoclasts after M-CSF and RANKL induction at 0, 2 and 4 d. Scale bar, 200 μm. **(D)** Immunofluorescence co-staining of MAGI1 (green) and F-actin (red) at 0, 2 and 4 days after RANKL induction. Scale bar, 100 μm; 50 μm (magnification). **(E)** SO-FG staining of the subchondral bone in the OA and RN parts from human osteoarthritic tibial plateau samples. RN = relatively normal part; OA = damaged osteoarthritic part. Scale bar, 1000 μm. **(F)** Immunofluorescence co-staining of MAGI1 and TRAP in subchondral bone of the OA and RN parts. Scale bar, 200 μm. **(G)** Quantitative analysis of MAGI1 intensity in subchondral bone of the OA and RN parts. n = 5. **(H)** SO-FG and TRAP staining to assess cartilage and subchondral bone damage in mice at 4 weeks after DMM surgery. Scale bar, 200 μm (upper), 100 μm (middle), 100 μm (bottom). **(I)** Immunofluorescence co-staining of MAGI1 (green) and TRAP (red) in tibial subchondral bone marrow at 4 weeks after DMM surgery. Scale bar, 200 μm. **(J, K)** Statistics of ratio of hyaline cartilage to calcified cartilage thickness, and quantification of $TRAP^{+}$ osteoclasts in subchondral bone marrow. n = 5. **(L)** Quantitative analysis of MAGI1 fluorescence intensity in subchondral bone marrow, n = 4. Error bars are means ± s.d., $^{*}P < 0.05$, $^{**}P < 0.01$, $^{***}P < 0.001$, by one-way ANOVA with several comparisons employing the Tukey method. Comparisons between two groups were performed using the two-tailed Student's *t*-test.

and RT-qPCR were used to detect the efficiency of transfection, which showed that siRNA#1 and siRNA#2 had the most significant transfection efficiency on MAGI1 knockdown (Supplementary Fig. S2). Therefore, siRNA#1 and siRNA#2 were selected for the subsequent experiments. TRAP staining showed that knockdown of MAGI1 significantly promoted the differentiation potential of osteoclasts (Fig. 2A and B). A number of reports have suggested that filopodia and filopodia-like protrusions participate in osteoclast fusion, osteoclast precursors recognize fusion partners by filopodia and establish dynamic connections between two cells before membrane fusion [29,33]. Thus, on day 4 of RANKL-induced osteoclasts, immunofluorescence co-labeling of MAGI1 and F-actin indicated the significantly promotion of filamentous pseudopod formation in the siMagi1 group compared to the siCtrl group (Fig. 2C and D). Meanwhile, F-actin rings used to assess osteoclast maturation were formed more after downmodulation of MAGI1 (Fig. 2E and F). In addition, we analyzed the expression of osteoclast-related genes using Magi1 siRNA#2, RT-qPCR results indicated that the expression of Acp5, c-Fos, Nfatc1, and Ctsk, was obviously up-regulated in the siMagi1 group (Fig. 2G). These data suggest that osteoclasts with MAGI1 knockdown have an enhanced capacity to differentiate.

3.3. Knockdown of MAGI1 in subchondral bone aggravates DMM-induced OA progression in a rat model

Osteoclast activity and bone remodeling rate were increased in the early stage of OA [41]. A rise in osteoclast activity can upset the balance between bone formation and resorption, causing a notable decrease in subchondral bone, which may further impact the initiation and development of OA [42]. To explore the impact of MAGI1 deficiency on OA progression in rats, we initially isolated BMDMs from the femoral and tibial bones of rats, followed by RANKL-induced differentiation into osteoclasts. We confirmed that MAGI1 gene had the same expression pattern in rats as it does during mouse osteoclast differentiation (Supplementary Fig. S3). Similarly, we transiently transfected rat BMDMs with Magi1 siRNA. RT-qPCR analysis revealed a significant reduction in MAGI1 expression following siRNA transfection, confirming the successful knockdown of MAGI1 in rat osteoclasts (Supplementary Fig. S4). Subsequently, we conducted DMM surgery to establish an OA model in rats and collected joint tissue samples for histological analysis (Fig. 3A). To investigate the effect of rAVV9 mediated shRNA against Magi1 in subchondral bone remodeling, we locally injected the Magi1 shRNA virus (rAAV9-U6-CMV-GFP-shMagi1) and the control (rAAV9-CMV-GFP) into the subchondral bone of DMM-induced OA rats to silence MAGI1 (Fig. 3B). Three weeks after the rAVV9 injection, the immunofluorescence detected the AAV9 expression in subchondral bone tissue (Fig. 3C). We next conducted the phenotypic analysis to explore how silencing MAGI1 in subchondral bone marrow affects the development of OA. TRAP staining revealed the low expression of MAGI1 in subchondral bone exhibited higher levels of TRAP-positive osteoclasts compared to the control group at 4-week post-DMM surgery (Fig. 3D and F). Micro-CT was used to analyze the microstructure alteration of the subchondral bone and to calculate the bone parameters. Compared with the control group, the subchondral bone microstructure damage was more serious in the AAV-shMagi1 group, in consistent with the increase in osteoclasts (Fig. 3E). Specifically, compared with the control group, there were decreases in BV/TV, Tb.N, Tb.Th, and an increase in Tb.Sp in the AAV-shMagi1 group at 4 weeks postoperatively (Fig. 3G–J). Then, SO-FG and H&E staining suggested that cartilage damage was more severe in the AAV-shMagi1 group than in the control group, which was reflected in the aggravated OARSI score (Fig. 3K and L). These results suggest that low expression of MAGI1 in subchondral bone promotes the formation of osteoclasts, leading to disturbance of subchondral bone homeostasis, thereby accelerating the pathological process of OA.

3.4. Suppressing MAGI1 expression in subchondral bone promotes vascularization, CGRP + innervation, and pain hypersensitivity

Increases in subchondral bone angiogenesis and pain are clinical symptoms of OA [43]. H-type vessels in subchondral bone is mainly mediated by PDGF-BB secreted by preosteoclasts, and abnormal H-type vessels is closely related to bone remodeling [11,44]. Besides, Netrin-1 secreted by osteoclasts is implicated in the recruitment and innervation of $CGRP^+$ nerve fibers, which mediates sensory nerve infiltration and pain in OA [16]. To determine whether knockdown of MAGI1 aggravated H-type angiogenesis and pain, we assessed the distribution of PDGF-BB, Netrin-1 and $CGRP^+$ nerve fibers in the subchondral bone marrow. Immunofluorescence demonstrated that increased PDGF-BB-positive cells in the AAV shMagi1 rats compared to the AAV-con rats 4 weeks post-DMM surgery (Fig. 4A and B). Netrin-1 and $CGRP^+$ sensory neurons that may mediate OA related pain were also significantly raised in the subchondral bone marrow of the AAV shMagi1 rats than in that of the AAV-con rats (Fig. 4A, B and Supplementary Fig. S5). Furthermore, we treated HUVECs with conditioned medium from osteoclast precursor cells of siMagi1 for tube formation assays, and the results indicated that the conditioned medium from osteoclast precursors of siMagi1 promoted the tube branch length and nodes compared to those cells of the siCtrl derived conditioned medium (Fig. 4C and D). Similarly, RT-qPCR also showed that siMagi1 promoted PDGF-BB gene expression in osteoclastic precursors (Supplementary Fig. S6). Clinical studies have found that individuals with OA have gait dysfunction, primarily in the form of slower gait speeds and shorter stride length [45,46]. Thus, we collected the footprints from rats and statistically analyzed the collected footprints for stride length and print area. Compared with the AAV-con group, the print area of footprint area was significantly reduced after knockdown of MAGI1, and there was no significant difference in the change of stride length (Fig. 4E and F). In summary, these results reveal the facilitating role of lower MAGI1 expression in osteoclastogenesis promotes PDGF-BB release and $CGRP^+$ sensory neuron recruitment, leading to increased angiogenesis and pain.

3.5. Overexpression of MAGI1 reduces osteoclastogenesis in vitro

Considering the positive effect of MAGI1 loss-of-function on osteoclastogenesis, overexpression of MAGI1 may be therapeutically important for treating OA. Thus, we used the MAGI1 overexpression plasmid to assess whether MAGI1 gain-of-function could inhibit osteoclastogenesis. Specifically, we extracted the primary BMDMs, transiently transfected with an overexpression plasmid of Magi1, RT-qPCR verified the overexpression efficiency (Supplementary Fig. S7). Then we performed the TRAP staining and found that MAGI1 overexpression notably inhibited osteoclast formation (Fig. 5A and B). In addition, we used immunofluorescence staining to analyze F-actin rings formation, which was found to be markedly impaired in osteoclasts with MAGI1 overexpression relative to the control group (Fig. 5C and D). Furthermore, RT-qPCR revealed that the expression of osteoclastogenesis marker genes was notably reduced at the mRNA level in the MAGI1 overexpression osteoclasts, including Acp5, c-Fos, Nfatc1, Ctsk, Atp6v0d2, and Dc-stamp (Fig. 5E). Overall, the results imply that MAGI1 negatively regulates the formation of osteoclasts.

3.6. MAGI1-mediated osteoclast fusion is regulated via inhibiting the RhoA/ROCK1/NF-κB pathway

MAGI1 acts as a scaffolding protein that interacts with a variety of signaling molecules and proteins involved in the cytoskeleton organization and stabilization. To further explore the mechanism of MAGI1 inhibiting osteoclast differentiation, we performed proteomic analyses to detect and identify the potential MAGI1 binding proteins. Based on the mass spectrometry data, we selected the top 20 potential binding proteins with high enrichment scores for graph. Among these candidate

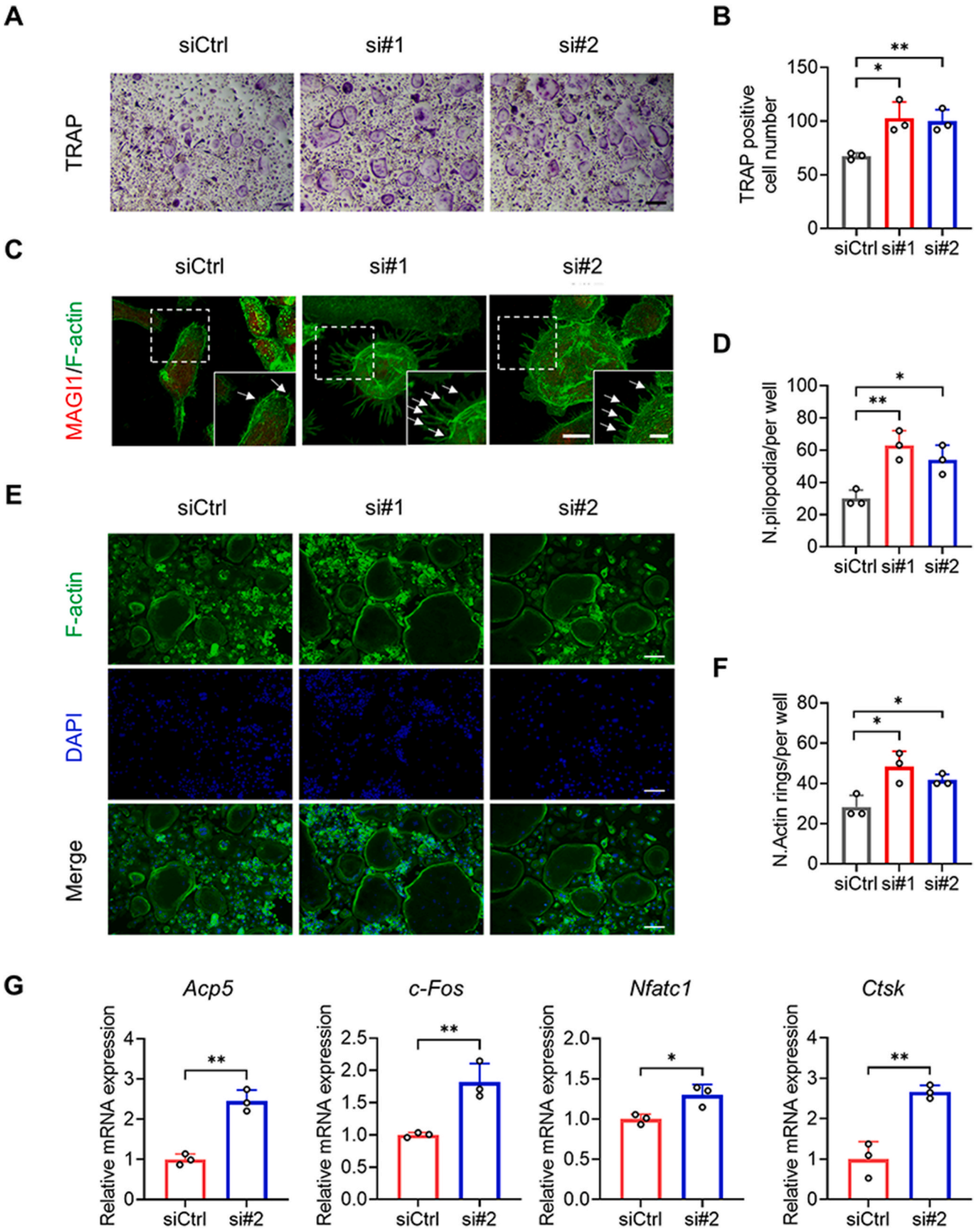

Fig. 2. MAGI1 is vital for osteoclast fusion *in vitro*. (A) TRAP staining was performed to detect the differentiation of osteoclasts on day 4. Scale bar, 200 μm. **(B)** Quantitative analysis of TRAP-positive cells number in per well. n = 3. **(C)** Immunofluorescence staining of F-actin and MAGI1 on day 3, and the filopodia formation was observed by fluorescence confocal microscopy. Scale bar, 200 μm; 100 μm (magnification). **(D)** Quantification of the filopodia. n = 3. **(E)** Immunofluorescence for F-actin rings formation on day 4. Scale bar, 100 μm. **(F)** Quantification of osteoclasts with F-actin rings per well. **(G)** RT-qPCR analyses of osteoclast-related gene expression including Acp5, c-Fos, Nfatc1, and Ctsk. n = 3. Error bars are means ± s.d., $^{*}P < 0.05$, $^{**}P < 0.01$, $^{***}P < 0.001$, by one-way ANOVA with several comparisons employing the Tukey method. Comparisons between two groups were performed using the two-tailed Student's *t*-test.

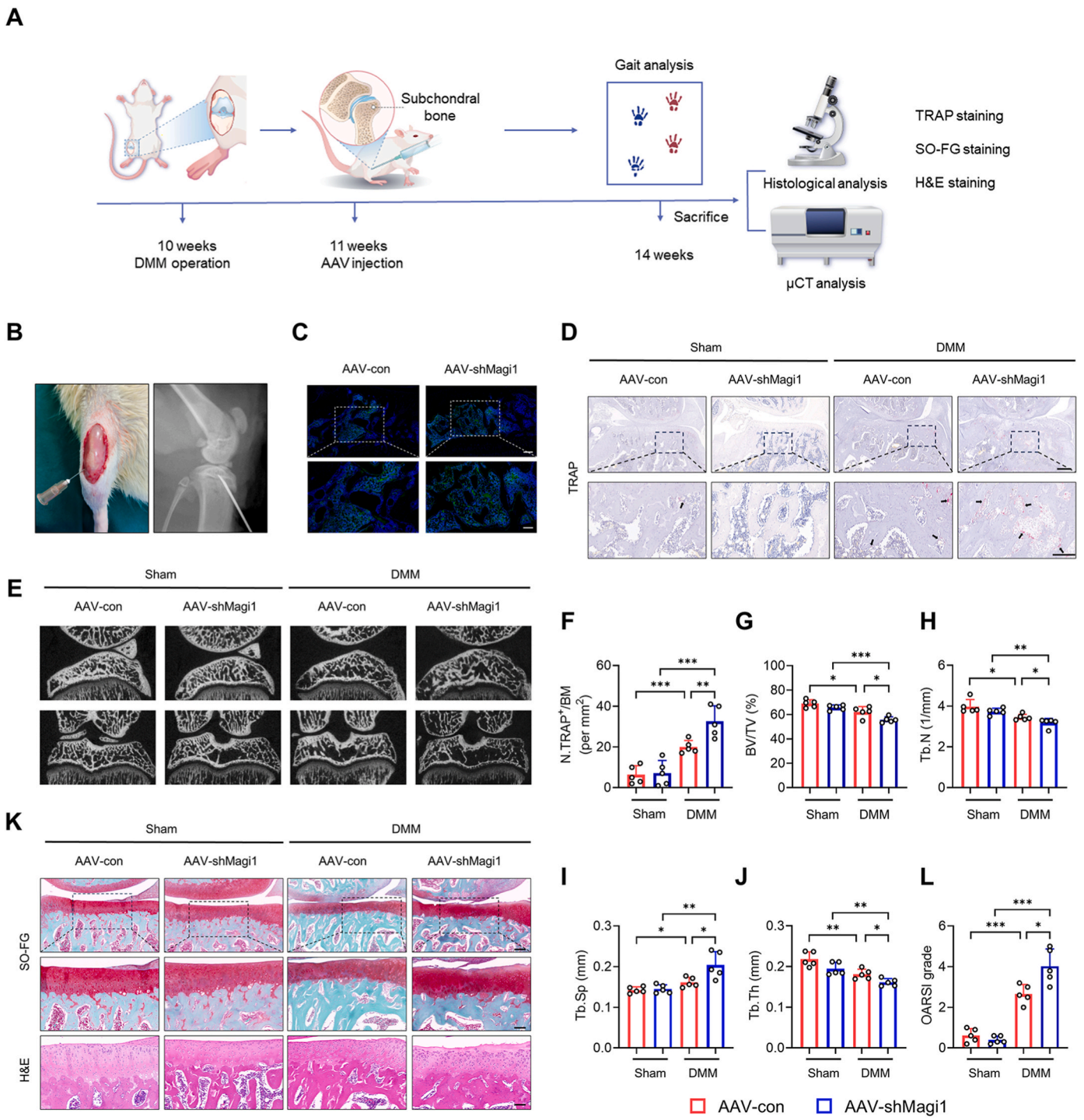

Fig. 3. Knockdown of MAGI1 promotes DMM-induced OA progression in a rat model. (A) Schematic illustration of the experimental design of the OA rat model. **(B)** A strategy for silencing MAGI1 expression by AAV9 injection into subchondral bone. **(C)** Immunofluorescence detected the efficiency of GFP expression in the subchondral bone of the AAV-con and AAV-shMagi1 groups. Scale bar, 200 μm (upper); 100 μm (bottom). **(D, F)** TRAP staining images of tibial subchondral bone in the AAV-shMagi1 and AAV-con groups at 4 weeks after DMM surgery, and quantitative analysis of $TRAP^{+}$ cells in subchondral bone marrow. n = 5. Scale bar, 500 μm (upper); 200 μm (bottom). **(E)** Micro-CT images of tibial subchondral bone in the AAV-shMagi1 and AAV-con groups at 4 weeks after DMM surgery. **(G–J)** Quantitative analysis of bone parameters of the tibia subchondral bone, including BV/TV, Tb.N., Tb.Sp. and Tb.Th. n = 5. **(K)** SO-FG staining (upper) and H&E staining (bottom) images in the AAV-shMagi1 and AAV-con groups at 4 weeks post-DMM surgery. Scale bar, 200 μm (upper); 100 μm (middle); 100 μm (bottom). **(L)** OARSI score based on SO-FG staining and H&E staining. n = 5. Error bars are means ± s.d., $^{*}P < 0.05$, $^{**}P < 0.01$, $^{***}P < 0.001$, by one-way ANOVA with several comparisons employing the Tukey method.

proteins, we were surprised to find that RhoA might interact with MAGI1 (Supplementary Fig. S8A). Studies have shown that MAGI1 promotes the activation of RhoA in endothelial cells [47]. RhoA activates Rho-associated coiled-coil containing protein kinase 1 (ROCK1) through phosphorylating ROCK1 downstream substrates, which has been recognized as a key regulator of the actin cytoskeleton [48], and an important participant in the formation of the actin rings of osteoclasts [49,50]. Subsequently, we validated this interaction through

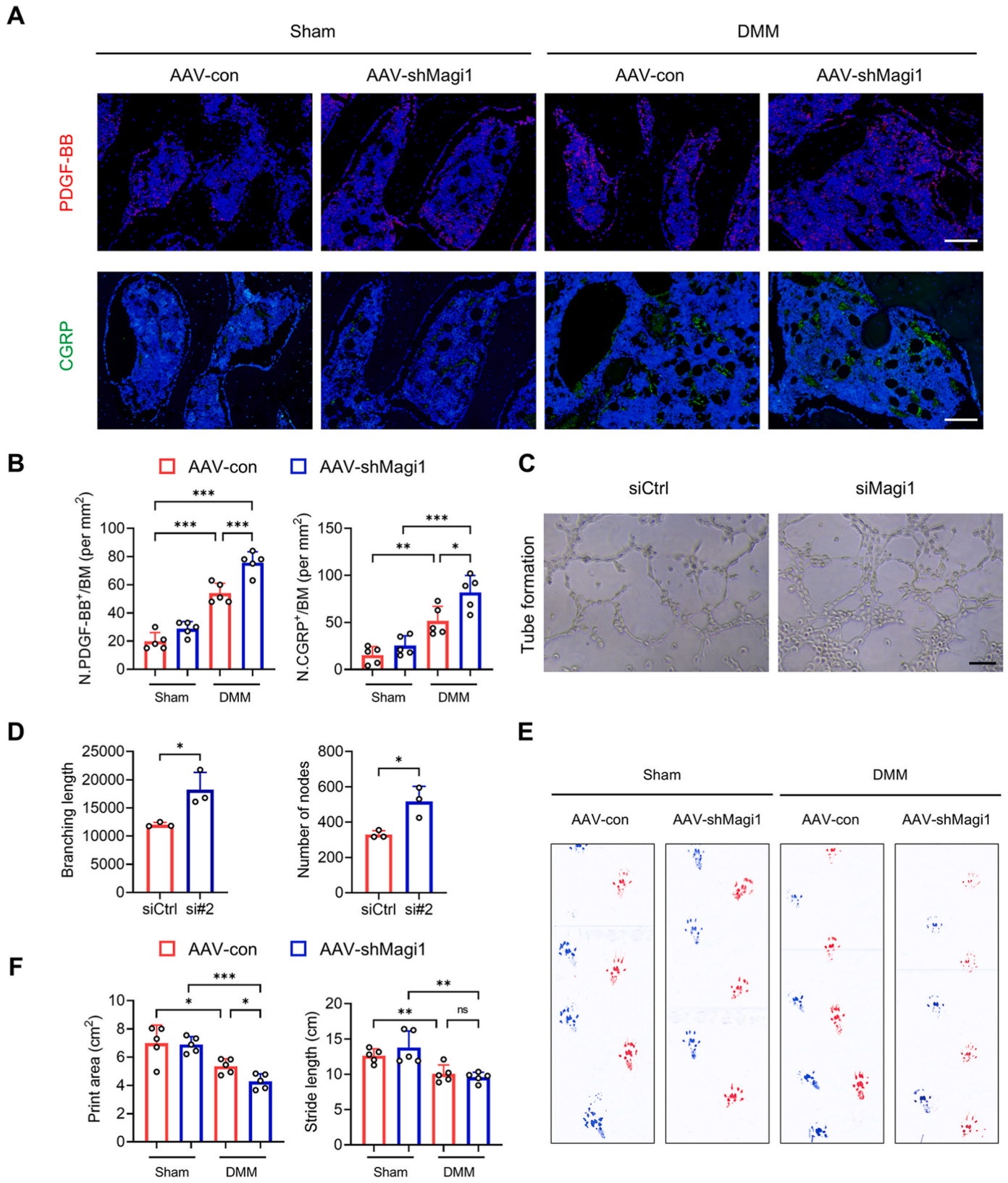

Fig. 4. Knockdown of MAGI1 aggravates subchondral bone vascularization and nerve invasion. (A) Tissue immunofluorescence staining of PDGF-BB (upper) and $CGRP^+$ nerve fibers (bottom) in the subchondral bone of the AAV-shMagi1 and AAV-control groups 4-weeks post-DMM surgery. Scale bar, 100 μm. **(B)** Quantitative analysis of PDGF-BB and $CGRP^+$ nerve fibers. n = 5. **(C)** Representative images of the HUVECs tube formation assay. Scale bar, 200 μm. **(D)** Quantitation of branching length and node numbers of HUVEC tubes. n = 3. **(E)** Footprint analysis of rats 4 weeks after DMM surgery. Modeling side in red, healthy side in blue. **(F)** Quantification of footprint stride length and footprint area, n = 5. Error bars are means ± s.d., $^*P < 0.05$, $^{**}P < 0.01$, $^{***}P < 0.001$, by one-way ANOVA with several comparisons employing the Tukey method. Comparisons between two groups were performed using the two-tailed Student's *t*-test.

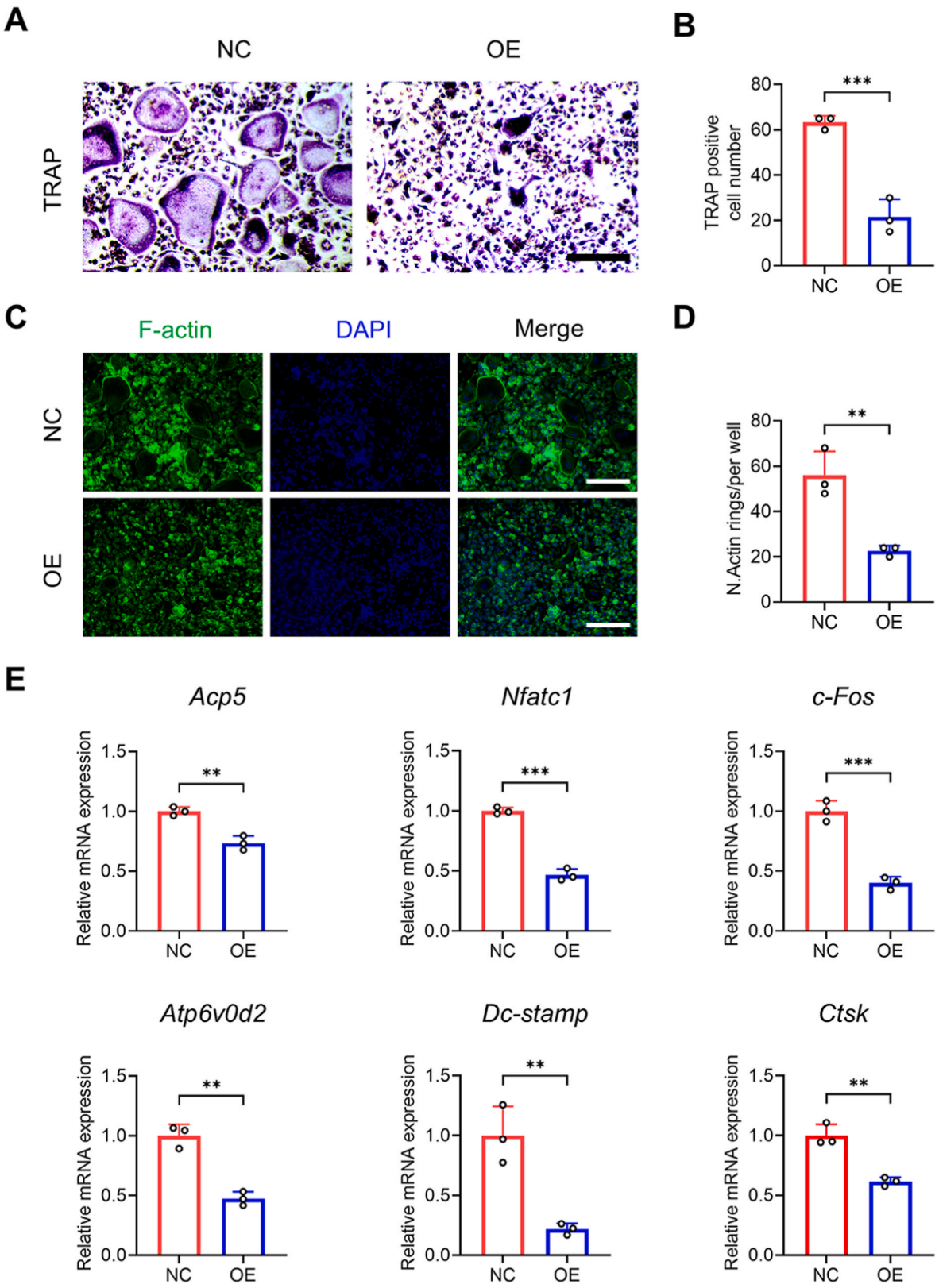

Fig. 5. Overexpression of MAGI1 in preosteoclasts suppresses osteoclastogenesis *in vitro.* (A) TRAP staining of osteoclasts derived from RANKL-treated BMDMs cells with overexpression of MAGI1 on 5–6 d. Scale bar, 200 μm. **(B)** Quantitative analysis of TRAP-positive cell number in per well. n = 3. **(C)** Actin ring structures of osteoclasts derived from RANKL-treated BMDMs with overexpression of MAGI1 on 5–6 d. Scale bar, 200 μm. **(D)** Quantitative analysis of actin rings in per well. n = 3. **(E)** RT-qPCR detected the osteoclast-related gene expression levels of Acp5, Nfatc1, c-Fos, Atp6v0d2, Dc-stamp, and Ctsk in the NC and OE-MAGI1 groups on 4 d n = 3. Error bars are means ± s.d., $^{*}P < 0.05$, $^{**}P < 0.01$, $^{***}P < 0.001$, by one-way ANOVA with several comparisons employing the Tukey method. Comparisons between two groups were performed using the two-tailed Student's *t*-test.

co-immunoprecipitation (CO-IP) assays. However, the CO-IP results indicated that MAGI1 did not directly interact with RhoA (Supplementary Fig. S8B). Next, we examined the expression changes of RhoA and its downstream signaling molecules following MAGI1 overexpression. The results demonstrated that MAGI1 overexpression significantly suppressed both the mRNA and protein expression levels of RhoA and its downstream effector, ROCK1 (Fig. 6A and B, and Supplementary Fig. S8C). NF-κB is a key signaling pathway that regulates osteoclast differentiation. Emerging studies show the expression of RhoA regulate the level of p-p65, indicating RhoA was upstream of NF-κB signaling and regulated NF-κB signaling in osteoclastogenesis [48,51,52]. Subsequently, western blotting revealed that MAGI1 inhibited p65 phosphorylation, leading to the downregulation of c-Fos expression (Fig. 6C, and Supplementary Fig. S8C). These findings suggest that MAGI1 may inhibit p65 phosphorylation by suppressing the RhoA/ROCK1 signaling pathway. To validate this hypothesis, we employed narciclasine (Narc), a RhoA agonist, for further investigation. BMDMs were treated with Narc at specified concentrations for 48 h, CCK8 assays revealed that Narc concentrations below 10 mM did not exhibit cytotoxicity on BMDMs (Supplementary Fig. S8D). Subsequently, 10 mM Narc was added to the MAGI1 overexpression group to rescue RhoA expression. RT-qPCR results demonstrated that Narc reversed the inhibitory effect of MAGI1 on ROCK1, as well as on the osteoclastic differentiation genes c-Fos and Ctsk (Fig. 6D). In addition, immunofluorescence showed that MAGI1 downregulated ROCK1 expression, which was significantly restored after Narc treatment (Fig. 6E and F). Then, we examined the nuclear translocation of p-p65. The immunofluorescence results indicated that the majority of p-p65 in the MAGI1 overexpression group was localized in the cytoplasm, while the addition of Narc significantly increased the RANKL-induced nuclear translocation of p-p65 (Fig. 6G and H). Finally, TRAP staining demonstrated that Narc partially restored the osteoclastogenic potential inhibited by overexpression of MAGI1 (Fig. 6I and J). These results confirm that MAGI1 inhibits osteoclast fusion by disrupting the RANKL-induced activation through RhoA/ROCK1/NF-κB pathway (see Fig. 7).

4. Discussion

In this study, we demonstrated that the scaffolding protein MAGI1 was significantly downregulated in both knee joint samples from OA patients and OA mouse models. Additionally, during *in vitro* osteoclast differentiation, the expression pattern of MAGI1 showed an inverse correlation with osteoclast marker genes. Functional studies revealed that MAGI1 knockdown not only enhanced osteoclastogenesis but also exacerbated subchondral bone microarchitecture deterioration, ultimately accelerating cartilage degeneration under pathological conditions. Conversely, MAGI1 overexpression significantly inhibited osteoclast differentiation. Mechanistic studies revealed that MAGI1 suppresses RANKL-induced p65 phosphorylation and inhibits osteoclast fusion in subchondral bone by inhibiting the RhoA/ROCK1 pathway.

Studies have shown that abnormal subchondral bone remodeling, including inflammation, angiogenesis, and innervation, plays a key role in the origin of OA pain [53]. Subchondral bone remodeling is a process in which old and damaged bone is replaced by new bone through osteoclast-mediated bone resorption and osteoblast-mediated bone formation, without altering the bone's shape. In the subchondral bone microenvironment, osteoclast-mediated bone resorption and osteoblast-mediated bone formation are coupled through endocrine and paracrine factors, inducing the migration and differentiation of their precursor cells [54,55]. During physiological remodeling, osteoclast-derived TGF-β and IGF-1 recruit mesenchymal stem cells (MSCs) to resorption pits, initiating bone formation [56,57], while synchronized angiogenesis further supports this process [58]. Notably, MSCs and endothelial cells (ECs) interact via secreted factors to modulate vascularization [59], with PDGF-BB from osteoclast precursors enhancing MSCs/ECs migration and angiogenesis [60,61]. Therefore, maintaining the homeostasis of the subchondral bone microenvironment is crucial for preventing the onset and progression of OA. Targeting osteoclast activity and the subchondral bone microenvironment to delay OA progression is now considered a potential therapeutic strategy.

Osteoclastogenesis is a sophisticated multi-step process tightly regulated by diverse molecular mechanisms and signaling pathways. Our findings demonstrate that MAGI1 expression is downregulated during osteoclast differentiation, exhibiting an inverse correlation with the gene expression profile characteristic of osteoclast formation. Furthermore, MAGI1 knockdown promotes the formation of filopodia and actin rings, thereby enhancing the subsequent processes of osteoclast fusion and differentiation. These results suggest that MAGI1 overexpression may suppress osteoclastogenesis, which is corroborated by our experimental data showing that *in vitro* overexpression significantly inhibits osteoclast formation. Therefore, targeting MAGI1 overexpression represents a potential therapeutic strategy for OA intervention. However, the MAGI1 gene sequence exceeds the packaging capacity of AAV vectors, limiting its efficient delivery for in vivo overexpression studies. To address this limitation, we propose the following alternative strategies in future studies: (1) developing small-molecule agonists targeting MAGI1; (2) designing recombinant proteins encoding key functional domains of MAGI1; (3) modulating upstream regulators or downstream effectors of MAGI1. In summary, the feasibility and efficacy of these alternative approaches require systematic validation and optimization in future studies.

Existing evidence indicates that TGF-β knockdown or its inhibition in subchondral bone alleviates the progression of OA [12,13], while angiogenesis suppression similarly exerts therapeutic effects [62]. Furthermore, NGF and Netrin-1 released by osteoclasts lead to innervation of subchondral bone sensory nerves in patients with OA, causing pain [16]. Additionally, an interesting finding has been proposed in research: the invasion of oxygen-rich H-type vessels into the subchondral bone disrupts the hypoxic environment of the entire joint [63]. Therefore, maintaining a hypoxic environment in the subchondral bone during the early stages of OA can help delay the progression of OA. However, as OA progresses, the use of anti-osteoclast drugs cannot reverse the formation of H-type vessels or the disruption of the hypoxic environment. At this stage, targeting HIF-1α in chondrocytes to maintain a hypoxic environment within the cartilage can help slow the progression of OA [63,64]. Our research primarily focuses on the early stages of OA. In this study, knockdown of MAGI1 in subchondral bone marrow promoted PDGF-BB production, and knockdown of MAGI1 *in vitro* also significantly promoted PDGF-BB expression. Besides, MAGI1 knocking down in osteoclasts promoted the expression of $CGRP^{+}$ sensory neurons in subchondral bone. In conclusion, our data suggest that inhibition of MAGI1 exerts a promotive effect on osteoclast activation, which promotes PDGF-BB release and $CGRP^{+}$ nerve fiber recruitment.

It has been suggested that MAGI1 promotes the activation of RhoA and (Ras - related C3 botulinum toxin substrate 1) Rac1 [47,65,66]. RhoA is a small G-protein that cycles between inactive GDP-bound and active GTP-bound states, and RhoGEFs activate RhoA by promoting the exchange of GDP for GTP [67]. In its active form, it binds directly to the Rho-binding domain of ROCK and initiate downstream signaling pathways. Therefore, we explored whether MAGI1 interacts with RhoA and thereby regulates RhoA activation. However, the results showed that MAGI1 does not directly interact with RhoA in osteoclasts. Next, we proceeded to investigate how MAGI1 controls the expression of RhoA and its downstream molecules. Currently, there is a wide range of studies on RhoA in osteoclasts. However, many opinions are conflicting. Some studies suggested that RhoA attenuates osteoclastogenesis by impairing the formation of actin rings in osteoclasts [50,68]. A study reported that a synergistic interaction between Rho and Cdc42 is required during actin rings formation in osteoclasts [49]. However, other studies have shown that RhoA promotes osteoclastogenesis. By conditionally knocking down RhoA in osteoclasts, it was shown that

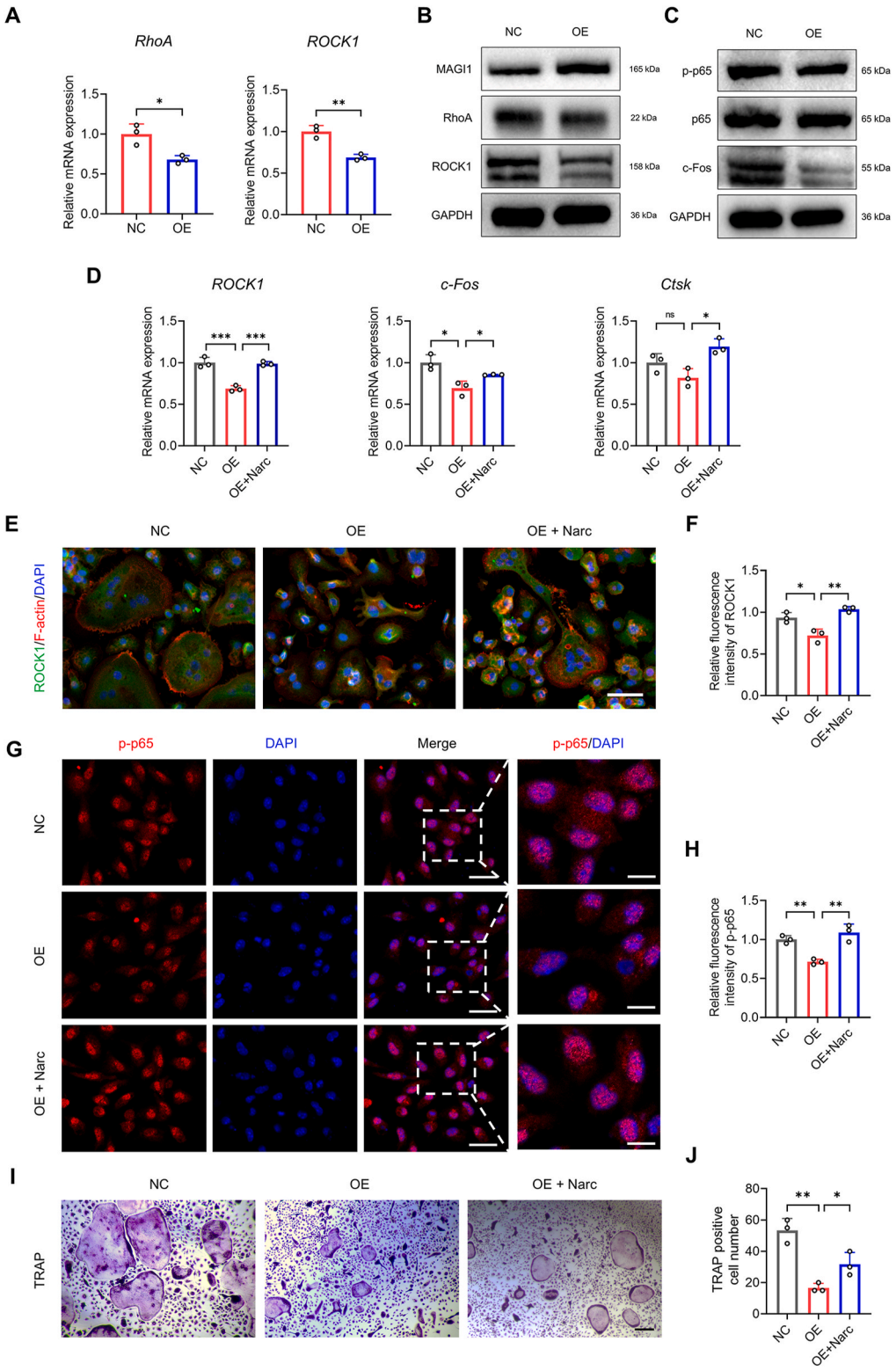

Fig. 6. Targeting MAGI1-RhoA-ROCK1 pathway regulate osteoclastogenesis. (A) RT-qPCR analysis of RhoA and ROCK1 mRNA levels following MAGI1 overexpression. n = 3. **(B)** Western blotting was used to detect the protein levels of RhoA and ROCK1. GAPDH served as the internal control. **(C)** Western blotting analysis for p-p65, p65, and c-Fos in the RANKL-treated BMDMs. GAPDH served as the internal control. **(D)** RT-qPCR analysis of the effect of Narc on ROCK1, c-Fos, and Ctsk after overexpression of MAGI1. n = 3. **(E, F)** Immunofluorescence staining of F-actin (red), ROCK1 (green), and nucleus (blue) with addition of Narc, and quantification of ROCK1 fluorescence. Scale bar, 25 μm. n = 3. **(G)** Immunofluorescence staining of p-p65 with Narc and without Narc. Scale bar, 25 μm (Left), 10 μm (Right). **(H)** Statistical analysis of relative fluorescence intensity of p-p65. n = 3. **(I)** TRAP staining was performed to detect the differentiation of osteoclasts with or without the Narc. Scale bar, 200 μm. **(J)** Quantitative analysis of TRAP-positive cell numbers in per well. n = 3. Error bars are means ± s.d., $^{*}P < 0.05$, $^{**}P < 0.01$, $^{***}P < 0.001$, by one-way ANOVA with multiple comparisons using the Tukey method. Comparisons between two groups were performed using the two-tailed Student's *t*-test.

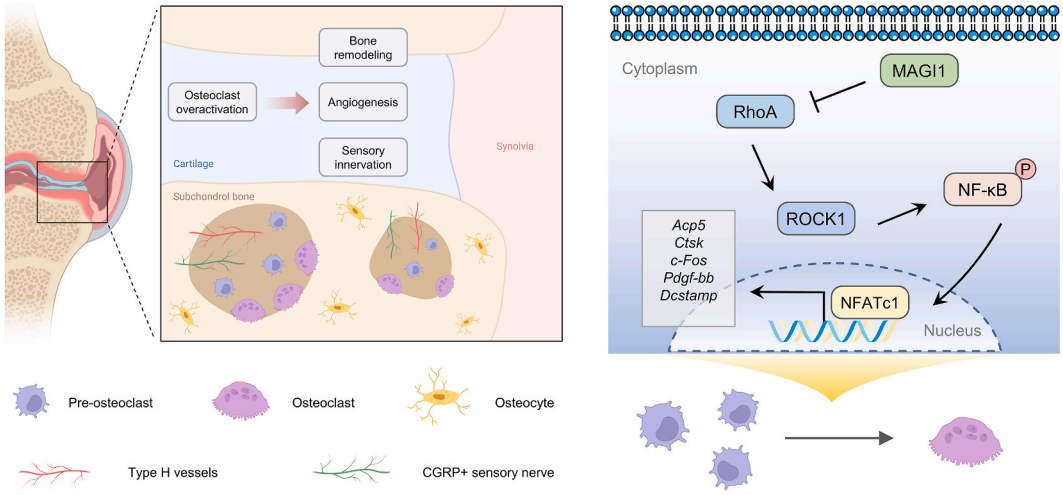

Fig. 7. Schematic model of mechanisms. During OA onset, overactivation of osteoclasts leads to subchondral bone remodeling, increased angiogenesis and sensory innervation invasion. During RANKL-induced osteoclast differentiation, high expression of MAGI1 in osteoclasts suppressed the RhoA/ROCK1 signaling pathway, which subsequently inhibited NF-κB-mediated osteoclastogenesis (Scheme created with BioRender).

RhoA deficiency inhibited the process of osteoclast differentiation via the Akt-mTOR-NFATc1 pathway [48]. Furthermore, in a study of Phi-targeted RhoA treatment in an osteoporosis model, it was demonstrated that both RhoA inhibitors and RhoA siRNA reduced osteoclast formation [52]. In our study, we revealed that MAGI1 overexpression suppressed the RhoA expression and its downstream molecule ROCK1, which in turn inhibited the p-p65 phosphorylation and reduced the osteoclast formation. Furthermore, agonists of RhoA partially restore the inhibitory effect on osteoclast formation after MAGI1 overexpression. Our study complements the expression pattern of RhoA in osteoclasts and suggests a novel mechanism for targeting MAGI1-RhoA-ROCK1 pathway regulate osteoclastogenesis.

It is worth investigating what prompts alterations in MAGI1 expression in osteoclasts. MAGI1 is an intracellular junction protein that colocalizes with a variety of intracellular molecules including paxillin, β3-integrin, and α-4-actinin [47]. It was discovered that MAGI1 interacts with β-catenin and E-cadherin to form complexes during the formation of cell-cell junctions, playing a role in regulating cell adhesion [24,69]. E-cadherin is primarily known as an adhesion junction protein that is suggested as fusion mediators for several cell types [70,71]. Research indicated that E-cadherin facilitates the migration and fusion of osteoclast precursors while also regulating osteoclast-specific gene expression [72]. Thus, we hypothesize that the recognition and fusion of mononuclear osteoclasts lead to alterations in E-cadherin expression in osteoclasts, which subsequently causes changes in MAGI1 expression. Further examination and validation are required in future studies.

In summary, the highlight of our study was the discovery that MAGI1 limits osteoclast fusion by inhibiting the RhoA/ROCK1 signaling pathway. Knockdown of MAGI1 in osteoclasts increased the number of subchondral bone osteoclasts, induced abnormal subchondral bone remodeling, and exacerbated OA progression. In addition, knockdown of MAGI1 significantly enhanced subchondral bone angiogenesis and elevated pain sensitivity. Therefore, our findings indicate that targeting MAGI1 and inhibiting the RhoA/ROCK1 signaling pathway plays a critical role in maintaining subchondral bone homeostasis and attenuating OA progression.

CRediT authorship contribution statement

Jing Zhang: Conceptualization, Methodology, Software, Writing – original draft. **Wenhui Hu:** Conceptualization, Investigation, Software, Writing – review & editing. **Yuheng Li:** Software, Investigation. **Fei Kang:** Methodology, Investigation. **Xuan Yao:** Investigation. **Jianmei Li:** Writing – review & editing, Formal analysis, Funding acquisition. **Shiwu Dong:** Resources, Writing – review & editing, Project administration, Funding acquisition.

Declaration of competing interest

The authors declare that they have no known competing financial interests or personal relationships that could have appeared to influence the work reported in this paper.

Acknowledgments

This work was financially supported by the Integration Project of NSFC Joint Fund for Regional Innovation and Development (U23A6008), the Key Program of National Natural Science Foundation of China (81930067), and the General Program of Natural Science Foundation of Chongqing (CSTB2023NSCQ-MSX0026).

Appendix. ASupplementary data

Supplementary data to this article can be found online at https://doi.org/10.1016/j.jot.2025.04.007.

References

[1] Martel-Pelletier J, Barr AJ, Cicuttini FM, Conaghan PG, Cooper C, Goldring MB, et al. Osteoarthritis. Nat Rev Dis Primers 2016;2:16072.
[2] Allen KD, Thoma LM, Golightly YM. Epidemiology of osteoarthritis. Osteoarthr Cartil 2022;30(2):184–95.
[3] Hügle T, Geurts J. What drives osteoarthritis?-synovial versus subchondral bone pathology. Rheumatology 2017;56(9):1461–71.
[4] Kloppenburg M, Berenbaum F. Osteoarthritis year in review 2019: epidemiology and therapy. Osteoarthr Cartil 2020;28(3):242–8.
[5] Nelson AE. Osteoarthritis year in review 2017: clinical. Osteoarthr Cartil 2018;26(3):319–25.
[6] Goldring SR. Alterations in periarticular bone and cross talk between subchondral bone and articular cartilage in osteoarthritis. Ther Adv Musculoskelet Dis 2012;4(4):249–58.
[7] Cui Z, Crane J, Xie H, Jin X, Zhen G, Li C, et al. Halofuginone attenuates osteoarthritis by inhibition of TGF-β activity and H-type vessel formation in subchondral bone. Ann Rheum Dis 2016;75(9):1714–21.
[8] Hu W, Chen Y, Dou C, Dong S. Microenvironment in subchondral bone: predominant regulator for the treatment of osteoarthritis. Ann Rheum Dis 2021;80(4):413–22.
[9] Hu Y, Chen X, Wang S, Jing Y, Su J. Subchondral bone microenvironment in osteoarthritis and pain. Bone Res 2021;9(1):20.
[10] Lacourt M, Gao C, Li A, Girard C, Beauchamp G, Henderson JE, et al. Relationship between cartilage and subchondral bone lesions in repetitive impact trauma-induced equine osteoarthritis. Osteoarthr Cartil 2012;20(6):572–83.

[11] Su W, Liu G, Liu X, Zhou Y, Sun Q, Zhen G, et al. Angiogenesis stimulated by elevated PDGF-BB in subchondral bone contributes to osteoarthritis development. JCI Insight 2020;5(8).
[12] Zhen G, Cao X. Targeting TGFβ signaling in subchondral bone and articular cartilage homeostasis. Trends Pharmacol Sci 2014;35(5):227–36.
[13] Zhen G, Wen C, Jia X, Li Y, Crane JL, Mears SC, et al. Inhibition of TGF-β signaling in mesenchymal stem cells of subchondral bone attenuates osteoarthritis. Nat Med 2013;19(6):704–12.
[14] Peng Y, Wu S, Li Y, Crane JL. Type H blood vessels in bone modeling and remodeling. Theranostics 2020;10(1):426–36.
[15] Mediero A, Ramkhelawon B, Perez-Aso M, Moore KJ, Cronstein BN. Netrin-1 is a critical autocrine/paracrine factor for osteoclast differentiation. J Bone Miner Res 2015;30(5):837–54.
[16] Zhu S, Zhu J, Zhen G, Hu Y, An S, Li Y, et al. Subchondral bone osteoclasts induce sensory innervation and osteoarthritis pain. J Clin Investig 2019;129(3):1076–93.
[17] Oliva C, Escobedo P, Astorga C, Molina C, Sierralta J. Role of the MAGUK protein family in synapse formation and function. Dev Neurobiol 2012;72(1):57–72.
[18] te Velthuis AJW, Admiraal JF, Bagowski CP. Molecular evolution of the MAGUK family in metazoan genomes. BMC Evol Biol 2007;7:129.
[19] Ide N, Hata Y, Nishioka H, Hirao K, Yao I, Deguchi M, et al. Localization of membrane-associated guanylate kinase (MAGI)-1/Bai-associated protein (BAP) 1 at tight junctions of epithelial cells. Oncogene 1999;18(54):7810–5.
[20] Wörthmüller J, Rüegg C. MAGI1, a scaffold protein with tumor suppressive and vascular functions. Cells 2021;10(6).
[21] Feng X, Jia S, Martin TA, Jiang WG. Regulation and involvement in cancer and pathological conditions of MAGI1, a tight junction protein. Anticancer Res 2014;34 (7):3251–6.
[22] Kantar D, Mur EB, Mancini M, Slaninova V, Salah YB, Costa L, et al. MAGI1 inhibits the AMOTL2/p38 stress pathway and prevents luminal breast tumorigenesis. Sci Rep 2021;11(1).
[23] Zaric J, Joseph JM, Tercier S, Sengstag T, Ponsonnet L, Delorenzi M, et al. Identification of MAGI1 as a tumor-suppressor protein induced by cyclooxygenase-2 inhibitors in colorectal cancer cells. Oncogene 2011;31(1):48–59.
[24] Sakurai A, Fukuhara S, Yamagishi A, Sako K, Kamioka Y, Masuda M, et al. MAGI-1 is required for Rap1 activation upon cell-cell contact and for enhancement of vascular endothelial cadherin-mediated cell adhesion. Mol Biol Cell 2006;17(2): 966–76.
[25] Ghimire K, Zaric J, Alday-Parejo B, Seebach J, Bousquenaud M, Stalin J, et al. MAGI1 mediates eNOS activation and NO production in endothelial cells in response to fluid shear stress. Cells 2019;8(5).
[26] Liang W, Feng R, Li X, Duan X, Feng S, Chen J, et al. A RANKL-UCHL1-sCD13 negative feedback loop limits osteoclastogenesis in subchondral bone to prevent osteoarthritis progression. Nat Commun 2024;15(1):8792.
[27] Sun H, Kaartinen MT. Transglutaminase activity regulates differentiation, migration and fusion of osteoclasts via affecting actin dynamics. J Cell Physiol 2018;233(9):7497–513.
[28] Chen Z-H, Wu J-J, Guo D-Y, Li Y-Y, Chen M-N, Zhang Z-Y, et al. Physiological functions of podosomes: from structure and function to therapy implications in osteoclast biology of bone resorption. Ageing Res Rev 2023;85:101842.
[29] Song RL, Liu XZ, Zhu JQ, Zhang JM, Gao Q, Zhao HY, et al. New roles of filopodia and podosomes in the differentiation and fusion process of osteoclasts. Genet Mol Res 2014;13(3):4776–87.
[30] Kong L, Wang B, Yang X, He B, Hao D, Yan L. Integrin-associated molecules and signalling cross talking in osteoclast cytoskeleton regulation. J Cell Mol Med 2020; 24(6):3271–81.
[31] Oikawa T, Oyama M, Kozuka-Hata H, Uehara S, Udagawa N, Saya H, et al. Tks5-dependent formation of circumferential podosomes/invadopodia mediates cell-cell fusion. J Cell Biol 2012;197(4):553–68.
[32] Blangy A, Bompard G, Guerit D, Marie P, Maurin J, Morel A, et al. The osteoclast cytoskeleton - current understanding and therapeutic perspectives for osteoporosis. J Cell Sci 2020;133(13).
[33] Takito J, Nakamura M. Heterogeneity and actin cytoskeleton in osteoclast and macrophage multinucleation. Int J Mol Sci 2020;21(18).
[34] Jang G, Lee SA, Hong JH, Park B-R, Kim DK, Kim CS. Chondroprotective effects of 4,5-dicaffeoylquinic acid in osteoarthritis through NF-κB signaling inhibition. Antioxidants 2022;11(3).
[35] Sun G-D, Chen Y, Zhou Z-G, Yang S-X, Zhong C, Li Z-Z. A progressive compression model of thoracic spinal cord injury in mice: function assessment and pathological changes in spinal cord. Neural Regen Res 2017;12(8):1365–74.
[36] Asahina M, Fujinawa R, Nakamura S, Yokoyama K, Tozawa R, Suzuki T. Ngly1 -/- rats develop neurodegenerative phenotypes and pathological abnormalities in their peripheral and central nervous systems. Hum Mol Genet 2020;29(10):1635–47.
[37] Hu W, Cai C, Li Y, Kang F, Chu T, Dong S. Farnesoid X receptor agonist attenuates subchondral bone osteoclast fusion and osteochondral pathologies of osteoarthritis via suppressing JNK1/2/NFATc1 pathway. FASEB J 2022;36(4):e22243.
[38] Sun X, Xie Z, Hu B, Zhang B, Ma Y, Pan X, et al. The Nrf2 activator RTA-408 attenuates osteoclastogenesis by inhibiting STING dependent NF-κb signaling. Redox Biol 2020;28:101309.
[39] Li X, Wang L, Huang B, Gu Y, Luo Y, Zhi X, et al. Targeting actin-bundling protein L-plastin as an anabolic therapy for bone loss. Sci Adv 2020;6(47).
[40] Feng N, Liang L, Fan M, Du Y, Chen C, Jiang R, et al. Treating autoimmune inflammatory diseases with an siERN1-nanoprodrug that mediates macrophage polarization and blocks toll-like receptor signaling. ACS Nano 2021;15(10): 15874–91.
[41] Wu Z, Yuan K, Zhang Q, Guo JJ, Yang H, Zhou F. Antioxidant PDA-PEG nanoparticles alleviate early osteoarthritis by inhibiting osteoclastogenesis and angiogenesis in subchondral bone. J Nanobiotechnol 2022;20(1):479.
[42] Fang H, Huang L, Welch I, Norley C, Holdsworth DW, Beier F, et al. Early changes of articular cartilage and subchondral bone in the DMM mouse model of osteoarthritis. Sci Rep 2018;8(1):2855.
[43] Hunter DJ, Bierma-Zeinstra S. Osteoarthritis. Lancet (London) 2019;393(10182): 1745–59.
[44] Xie H, Cui Z, Wang L, Xia Z, Hu Y, Xian L, et al. PDGF-BB secreted by preosteoclasts induces angiogenesis during coupling with osteogenesis. Nat Med 2014;20(11): 1270–8.
[45] Broström EW, Esbjörnsson A-C, von Heideken J, Iversen MD. Gait deviations in individuals with inflammatory joint diseases and osteoarthritis and the usage of three-dimensional gait analysis. Best Pract Res Clin Rheumatol 2012;26(3):409–22.
[46] Constantinou M, Barrett R, Brown M, Mills P. Spatial-temporal gait characteristics in individuals with hip osteoarthritis: a systematic literature review and meta-analysis. J Orthop Sports Phys Ther 2014;44(4). 291-B7.
[47] Alday-Parejo B, Ghimire K, Coquoz O, Albisetti GW, Tamò L, Zaric J, et al. MAGI1 localizes to mature focal adhesion and modulates endothelial cell adhesion, migration and angiogenesis. Cell Adhes Migrat 2021;15(1):126–39.
[48] Wang J, Xu C, Zhang J, Bao Y, Tang Y, Lv X, et al. RhoA promotes osteoclastogenesis and regulates bone remodeling through mTOR-NFATc1 signaling. Mol Med 2023;29(1):49.
[49] Chellaiah MA. Regulation of actin ring formation by rho GTPases in osteoclasts. J Biol Chem 2005;280(38):32930–43.
[50] Mizoguchi F, Murakami Y, Saito T, Miyasaka N, Kohsaka H. miR-31 controls osteoclast formation and bone resorption by targeting RhoA. Arthritis Res 2013;15 (5):R102.
[51] Wang X, Ji L, Wang J, Liu C. Matrix stiffness regulates osteoclast fate through integrin-dependent mechanotransduction. Bioact Mater 2023;27:138–53.
[52] Zhang J, Jiang T, Zhang Y, Yang K, Zhao Y, Zhou Q, et al. Phillygenin prevents osteoclast differentiation and bone loss by targeting RhoA. Phytother Res 2024;38 (4):1863–81.
[53] Qin W, Gao J, Yan J, Han X, Lu W, Ma Z, et al. Microarray analysis of signalling interactions between inflammation and angiogenesis in subchondral bone in temporomandibular joint osteoarthritis. Biomater Transl 2024;5(2):175–84.
[54] Del Fattore A, Teti A, Rucci N. Bone cells and the mechanisms of bone remodelling. Front Biosci (Elite Ed) 2012;4(6):2302–21.
[55] Sims NA, Martin TJ. Coupling the activities of bone formation and resorption: a multitude of signals within the basic multicellular unit. BoneKEy Rep 2014;3:481.
[56] Tang Y, Wu X, Lei W, Pang L, Wan C, Shi Z, et al. TGF-beta1-induced migration of bone mesenchymal stem cells couples bone resorption with formation. Nat Med 2009;15(7):757–65.
[57] Xian L, Wu X, Pang L, Lou M, Rosen CJ, Qiu T, et al. Matrix IGF-1 maintains bone mass by activation of mTOR in mesenchymal stem cells. Nat Med 2012;18(7): 1095–101.
[58] Ulici V, Hoenselaar KD, Agoston H, McErlain DD, Umoh J, Chakrabarti S, et al. The role of Akt1 in terminal stages of endochondral bone formation: angiogenesis and ossification. Bone 2009;45(6):1133–45.
[59] Nassiri SM, Rahbarghazi R. Interactions of mesenchymal stem cells with endothelial cells. Stem Cell Dev 2014;23(4):319–32.
[60] Kreja L, Brenner RE, Tautzenberger A, Liedert A, Friemert B, Ehrnthaller C, et al. Non-resorbing osteoclasts induce migration and osteogenic differentiation of mesenchymal stem cells. J Cell Biochem 2010;109(2):347–55.
[61] Wang H, Yin Y, Li W, Zhao X, Yu Y, Zhu J, et al. Over-expression of PDGFR-β promotes PDGF-induced proliferation, migration, and angiogenesis of EPCs through PI3K/Akt signaling pathway. PLoS One 2012;7(2):e30503.
[62] Lu J, Zhang H, Cai D, Zeng C, Lai P, Shao Y, et al. Positive-Feedback regulation of subchondral H-type vessel formation by chondrocyte promotes osteoarthritis development in mice. J Bone Miner Res 2018;33(5):909–20.
[63] Zhang H, Wang L, Cui J, Wang S, Han Y, Shao H, et al. Maintaining hypoxia environment of subchondral bone alleviates osteoarthritis progression. Sci Adv 2023;9(14):eabo7868.
[64] Zhang K, Fu W. HIF-1α: linking subchondral bone and cartilage as a therapeutic target in osteoarthritis. Biomater Transl 2024;5(1):89–91.
[65] Dobrosotskaya IY. Identification of mNET1 as a candidate ligand for the first PDZ domain of MAGI-1. Biochem Biophys Res Commun 2001;283(4):969–75.
[66] Kimura R, Ishida T, Kuriyama M, Hirata K-i, Hayashi Y. Interaction of endothelial cell-selective adhesion molecule and MAGI-1 promotes mature cell-cell adhesion via activation of RhoA. Genes Cells 2010;15(4):385–96.
[67] Gu J, Yang Z, Yuan L, Guo S, Wang D, Zhao N, et al. Rho-GEF trio regulates osteoclast differentiation and function by Rac1/Cdc42. Exp Cell Res 2020;396(1): 112265.
[68] Wu M, Chen W, Lu Y, Zhu G, Hao L, Li Y-P. Gα13 negatively controls osteoclastogenesis through inhibition of the Akt-GSK3β-NFATc1 signalling pathway. Nat Commun 2017;8:13700.
[69] Dobrosotskaya IY, James GL. MAGI-1 interacts with beta-catenin and is associated with cell-cell adhesion structures. Biochem Biophys Res Commun 2000;270(3): 903–9.

[70] Ishikawa A, Omata W, Ackerman WE, Takeshita T, Vandré DD, Robinson JM. Cell fusion mediates dramatic alterations in the actin cytoskeleton, focal adhesions, and E-cadherin in trophoblastic cells. Cytoskeleton (Hoboken) 2014;71(4):241–56.

[71] Van den Bossche J, Malissen B, Mantovani A, De Baetselier P, Van Ginderachter JA. Regulation and function of the E-cadherin/catenin complex in cells of the monocyte-macrophage lineage and DCs. Blood 2012;119(7):1623–33.

[72] Fiorino C, Harrison RE. E-cadherin is important for cell differentiation during osteoclastogenesis. Bone 2016;86:106–18.